Sequential shape-and-solder-directed self-assembly of functional microsystems

Wei Zheng*, Philippe Buhlmann†, and Heiko O. Jacobs*‡

Departments of *Electrical and Computer Engineering and †Chemistry, University of Minnesota, 200 Union Street SE, Minneapolis, MN 55455

Edited by George M. Whitesides, Harvard University, Cambridge, MA, and approved July 23, 2004 (received for review June 21, 2004)

We demonstrate the fabrication of packaged microsystems that contain active semiconductor devices and passive components by using a directed self-assembly technique. The directed self-assembly is accomplished by combining geometrical shape recognition with site-specific binding involving liquid solder. Microfabricated components with matching complementary shapes, circuits, and liquid solder-coated areas were suspended in ethylene glycol and agitated by using a turbulent liquid flow to initiate the self-assembly. Microsystems were obtained by sequentially adding components of different types. Six hundred AlGaInP/GaAs light-emitting diode segments with a chip size of 200 μm were assembled onto device carriers with a yield of 100% in 2 min. Packaged light-emitting diodes formed with yields exceeding 97% as a result of two self-assembly steps in 4 min. This self-assembly procedure, based on geometrical shape recognition and subsequent binding to form mechanical and electrical connections, provides a high distinguishing power between different components and a route to nonrobotic parallel assembly of electrically functional hybrid microsystems in three dimensions.

The construction of man-made artifacts such as cell phones and computers relies on robotic assembly lines that place, package, and interconnect a variety of devices that have macroscopic (>1 mm) dimensions (1). The size of such systems could be reduced by orders of magnitude if microscopic building blocks could be assembled in three dimensions (2). Conventional robotic methods and assembly lines, however, fail because of the difficulty in building machines that can economically manipulate components in three dimensions that are only micrometers in size (3). At another extreme, nature forms materials, structures, and living systems by self-assembly on a molecular length scale (4, 5). The employment of self-assembly to assemble functional microsystems that contain components out of different materials, however, has been challenging (6). Previous studies focused on aggregates containing two different components (7) as well as linear (8), planar (9–13), and three-dimensional arrays (14) that were built by repetitions of one component type.

Here we present a directed self-assembly method to realize multicomponent, multimaterial, three-dimensional microsystems. The method that we refer to as sequential shape-and-solder-directed self-assembly (SSSDS) combines aspects of shape-directed self-assembly with aspects of liquid solder-directed self-assembly. The self-assembly process uses geometrical shape recognition (7, 9) to identify different components and subsequent bond formation between liquid solder and metal-coated areas to form mechanical and electrical connections (12). Conceptually, SSSDS is different from earlier work in the sense that heterogeneous microsystems are built by sequentially adding different types of components to the assembly solution. SSSDS is tailored to enable the parallel assembly of microsystems that contain more than two nonidentical parts made from different materials. Each assembly sequence increases the complexity of the three-dimensional assembly. This concept is similar to the formation of heterodimers, trimers, and higher aggregates in biology and chemistry. It is different, however, in the sense that every component type provides a different functionality to the electrically interconnected assembly. Multicomponent microsystems are formed by sequentially adding parts to the assembly solution.

The dimensions ($\approx$200 μm) of the micro- and optoelectronic device segments that are used in this investigation are $\approx$15 times smaller than those used in current robotic assembly lines (3), $\approx$40 times smaller than those of previous solder-based self-assemblies (8, 14), and the same as those used in shape-directed fluidic self-assembly that assemble components on planar surfaces (9, 10). We demonstrate the assembly of 600 AlGaInP/GaAs light-emitting diodes (LEDs) onto device carriers in 2 min without defects and the assembly of packaged microsystems by sequentially adding parts to the assembly solution.

Materials and Methods

The experimental strategy to assemble and package microsystems is illustrated in Fig. 1. Each microsystem is formed by using three components, a semiconductor device segment, a silicon carrier, and a Pyrex glass encapsulation unit, with distinct complementary three-dimensional shapes, circuits, solder patterns, and copper metallization. We used LEDs as device segments to construct a system where the functionality can be tested visually. The illustration shows the experimental strategy for the LEDs, unpackaged cubic AlGaInP/GaAs LED segments with a side length of 200 μm (TK508DR, Tyntek, Hsinchu City, Taiwan). The chips had two contacts: a small circular anode on the front and a large square cathode covering the back.

The self-assembly and packaging is a two-step process: (*i*) chip-on-carrier assembly and (*ii*) chip encapsulation. To host, protect, and electrically connect the LEDs, we fabricated silicon carrier units using 280-μm-thick ⟨100⟩ silicon wafers (Virginia Semiconductor, Fredericksburg, VA). The procedure to fabricate the device carriers, circuits, and patterned solder drops on the three-dimensionally shaped units is described in *Supporting Text*, which is published as supporting information on the PNAS web site. Each silicon carrier provided a target site, a 200-μm-deep tapered opening, that fits one LED chip at a time. We integrated a binding site, a 200-μm-wide square solder-coated area, in the center of the opening for the attachment of the LED chips. During the first self-assembly step, the surface of the liquid solder wets and binds to the gold-coated cathode on the back side of the LEDs. The minimization of the free surface area of the liquid solder drives the assembly into a stable, aligned position. The solder also provides the electrical connection to operate the device and the mechanical bond required to hold the assembly together.

To protect the assembled LED segments and complete the electrical connections, we fabricated encapsulation units out of 500-μm-thick Pyrex wafers (Corning 7740, Universitywafer, Boston; see *Supporting Text*). Each encapsulation unit carried a 200-μm-deep tapered opening in the center to recognize the

This paper was submitted directly (Track II) to the PNAS office.

Abbreviations: SSSDS, sequential shape-and-solder-directed self-assembly; LED, light-emitting diode.

‡To whom correspondence should be addressed. E-mail: hjacobs@ece.umn.edu.

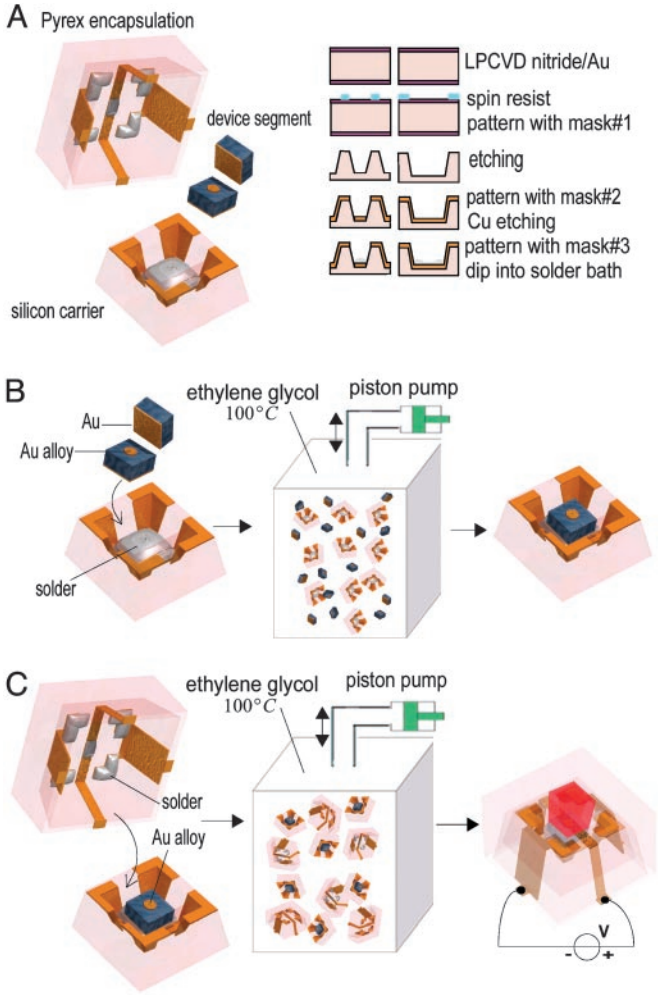

Fig. 1. Fabrication strategy to assemble and package integrated semiconductor devices by SSSDS. (*A*) Layout of the self-assembly components: carrier, device, and encapsulation unit that are fabricated by surface micromachining and etching. The illustrated device segment is an LED that has two contacts: a small circular anode on the front, and a large square cathode covering the back. The silicon carrier has a solder-coated area in a tapered opening to host a single semiconductor device segment. The encapsulation unit has five solder-coated copper areas inside a tapered opening to connect to corresponding contact pads on the device and carrier. LPCVD, low-pressure chemical vapor deposition. (*B* and *C*) Chip-on-carrier assembly (*B*) and chip encapsulation (*C*) in an ethylene glycol solution at a temperature of 100°C, where the solder is liquid. The components that are agitated by using a piston pump self-assemble and form a three-dimensional circuit path between device layers that allows testing in a surface-mount device configuration.

assembled LEDs during the encapsulation process and to distinguish between encapsulation units themselves. Each opening exposed five solder-coated areas to wet and bind to correspondingly shaped gold-coated areas on the LED and carrier during the second self-assembly step (see Fig. 1*C*).

Previous solder-based self-assembly systems used a suspension of components in water. To accomplish self-assembly, all surfaces must be free from contamination by metal oxides. This is typically accomplished by adding small concentrations of acetic acid (pH 2.5) to the assembly solution. This process, however, results in the oxidative dissolution of the solder itself because of two processes: $4M + 4nH^+ + nO_2 \rightarrow 4M^{n+} + 2nH_2O$ and $2M + 2nH^+ \rightarrow 2M^{n+} + nH_2$. As a consequence, wetting of the copper-binding sites with the solder becomes impaired. For example, for a solder-coated area 100 μm in size we notice a clear reduction in its wetting properties after 3 min. Deoxygenating the aqueous self-assembly solution by bubbling N_2 through it did not solve this problem. Another limitation of water is its low boiling point, which prohibits the use of high-melting point solders.

A number of alternatives to water as the self-assembly solvent were considered. Such a solvent needs to have a high boiling point and must not react with the solder, copper, glass, silicon, and the photoresist. It must dissolve the acid required to remove surfaces oxides from solder pads and copper contacts, and it should not react with this acid. To avoid contamination of the solder and copper surfaces with salts, this solvent must also dissolve the metal salts that form by the reaction of the acid with the metal oxides and the metals. The self-assembly solvent should wet the components to prevent the formation of trapped air bubbles in recesses, such as the tapered opening in the device carriers, because air bubbles interfere with the self-assembly process. Also, a too high solvent viscosity adversely affects the turbulent flow and must be avoided. It appears that ethylene glycol and several of its derivatives may fulfill these requirements. In this study, all self-assembly steps were performed in ethylene glycol at 100°C, where the solder (Y-LMA-117, Small Parts, Miami Lakes, FL) is molten. The ethylene glycol solution was made slightly acidic (pH 2.5) with sulfuric acid because its anions do not adsorb to metal surfaces, as would be the case for anions of several other mineral acids. Because ethylene glycol has a boiling point of 197°C, it allows the use of high-melting-point solders.

Previous research that focused on the formation of three-dimensional assemblies used different forms of tumbling (8, 14) and stirring (15) to agitate components with densities similar to the density of the self-assembly solution. We did not succeed in agitating the Si and GaAs semiconductor devices by using these methods because these materials have densities >3 times as large as the densities of water or ethylene glycol. Instead we built a turbulent pulsating flow system to provide a strong and reproducible form of agitation. The use of a turbulent flow is particularly suitable to agitate components with different length scales because the drag force in a liquid flow and the capillary force between two components follow the same scaling laws: both scale with the area. We also tested the agitation of the components by shaking (12) vials manually; however, the results were less reproducible. The turbulent pulsating flow was created by using a piston pump (PM6014, Fluid Metering, Syosset, NY) that expels and retracts liquid through a 2-mm-diameter nozzle submerged in the assembly solution. The amount and frequency of liquid that is cycled back and forth can be adjusted between 1 and 1.5 ml, and between 0 and 10 Hz, respectively. The assembly was carried out inside a rectangular glass container (12 mm on each side and 45 mm high) filled with 4.5 ml of ethylene glycol and immersed in an oil bath heated to 150°C.

Results and Discussion

Fig. 2 illustrates the experimental realization of the two-step, chip-on-carrier assembly and chip encapsulation process. For the chip-on-carrier assembly, we added 3,000 LED chips and 600 carrier units into the heated assembly solution and agitated the pieces by using the turbulent liquid flow. We obtained a yield of 100%, that is, all 600 carriers had captured an LED device segment, in 2 min. This experiment was reproduced six times; the yields were always >97%. The assembly speed and yield were influenced by two key parameters: the level of agitation and the number of available excess LEDs. The assembly speed increased with the level of agitation and reached a maximum when extracting and injecting 1.0 ml into the volume at a cycling rate of 3 Hz. A higher level of agitation (5 Hz, 1.0 ml) caused damage to assembled components because of component impaction. The assembly speed also increased with the number of excess LEDs:

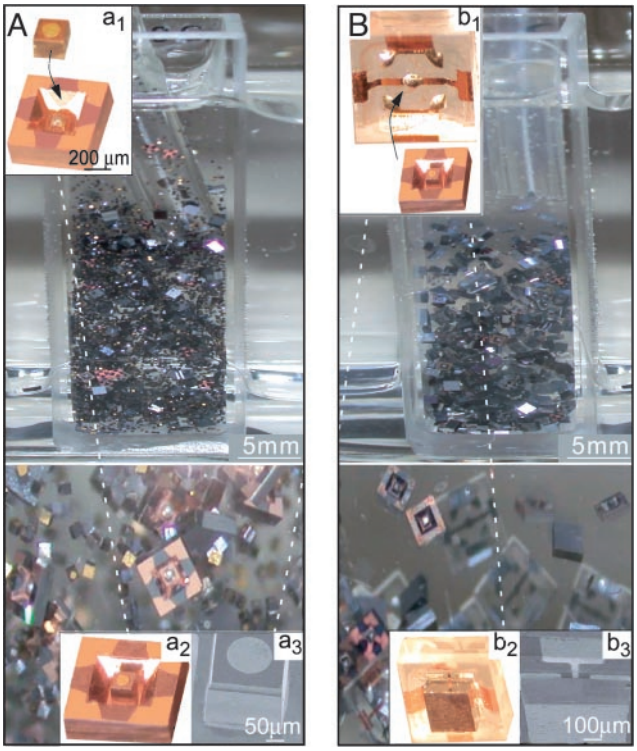

Fig. 2. Experimental realization of LED chips that were assembled and packaged by SSSDS. (*A* and *B*) Photographs (*Upper*) and micrographs (*Lower*) of the chip-on-carrier assembly and chip encapsulation. *Insets* show device components before (a_1 and b_1) and after (a_2 and b_2) each assembly step. The scanning electron micrographs (a_3 and b_3) illustrate the alignment between components.

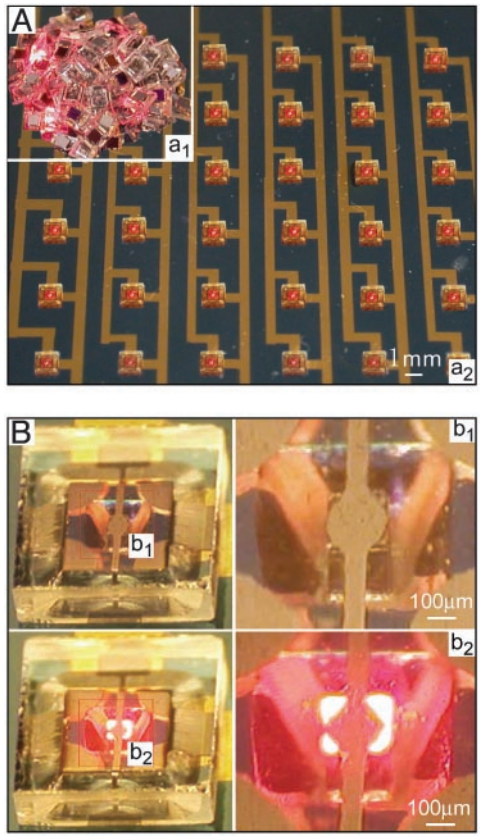

Fig. 3. Testing of LED chips that have been assembled and packaged by SSSDS. (*A*) Photograph of a cluster of 200 encapsulated devices that were assembled by the self-assembly process (a_1) and test of an array of LEDs that are mounted by hand on a printed circuit board (a_2). (*B*) Close-up photographs of the LED assemblies in the OFF (b_1) and ON (b_2) state, visualizing the formation of three-dimensional circuit paths between the different device layers and the printed circuit board. Boxed areas in *Left* are enlarged 3.2× in *Right*.

with 1,500 LEDs and 600 carriers in the assembly solution all carriers captured an LED in 6 min; with 3,000 LEDs it took 2 min to complete the self-assembly.

To prepare for the encapsulation process, we removed the excess LEDs by filtration through a 500-μm mesh filter and addition of 200 encapsulation units to the assembly container. Excess LEDs that were used to increase the assembly speed were reused in a later run. The yield of the encapsulation process was 97%, which means that 3% of the devices did not function as expected. We tested the functionality by hand mounting the devices on a printed circuit board and applying a potential of 2.1 V to the contact pads (Fig. 3). We reproduced the self-encapsulation process several times and found that variations in the height of up to $\approx$20 μm, and lateral misfits between the anode of the LEDs and the top electrode of up to $\approx$40 μm, were tolerated; beyond those limits the devices would not function. Small deviations were compensated by the reflow of solder and the repositioning of the LED, carrier, and encapsulation units. Deviations from the permissible range of sizes and positions resulted from variations in the size of the LEDs ($\approx$30 μm), and shape, thickness, and location of the solder-coated areas. In some cases we also found solder-based areas on the components that were only partially coated with solder, and components with partially detached metal areas as a source of defects. The overall yield of the process is currently 97% and can be increased by further removing the imperfection in the manufacturing of the components. These defects are not inherent to the self-assembly process itself, but were caused by imperfections in the manufacturing of the components.

Defects inherent to self-assembly processes are most commonly related to local energy minima in the space of possible conformations or to an insufficient overall energy minimum representing a stable assembly under agitation. We were able to remove local energy minima and associated defects completely by introducing and optimizing the complementary shapes. First carrier designs, for example, had truncated pyramidal openings that were three times as large as the LED device segments. As a result we found two device segments that assembled on a single receptor. We have removed such defects by reducing the size of the opening on the device carrier. We also optimized the overall energy minima by changing the size and shape of the solder-coated areas and the metallic binding sites on the device components. Early designs for the encapsulation units could not sustain high levels of agitation; defects were created by component impaction removing previously assembled LEDs and encapsulation units from the carriers. Fast and stable assemblies were accomplished by increasing the binding sites to cover more than 40% of the surface. The symmetry of the design influences the speed of the self-assembly process as well. The presented design has a fourfold symmetry and assembled faster than designs that had a twofold symmetry.

Conclusions

In summary, we demonstrated the self-assembly and packaging of microsystems by combining geometrical shape recognition with site-specific wetting and binding involving liquid solder. The multicomponent microsystems formed by sequentially adding parts to the assembly solution. Our technique enables assembling

heterogeneous microsystems in three dimensions and connecting them electrically, where the shape provides the ability to recognize a different component, and where the solder provides both the driving force and the electrical and mechanical connections.

We conclude that the combination of sequentially adding different types of components, geometrical shape recognition, and solder-directed self-assembly provides a greater flexibility in the design and manufacturing of electrically functional devices than previous strategies that focused on a single concept. Moreover, the components can be tailored to form microsystems with a minimum number of defects. The defect level in self-assembly appears to be a function of the distribution of the energy minima in the space of possible conformations and the level of agitation. SSSDS increases the ability to tailor the energy minima distribution. Local energy minima can be removed and a single allowable position can be defined which, we believe, is difficult to realize without combining the three concepts.

It remains to be seen whether SSSDS provides a practical alternative to conventional robotic assembly lines or wafer-to-wafer transfer techniques. The advantage of SSSDS and self-assembly in general over conventional robotic methods is that it is highly parallel. As a result, a reduction in the assembly costs can be expected when large quantities are needed. It might also be useful in applications where only small quantities of systems need to be realized and where the large capital investment of acquiring and maintaining a robotic assembly line cannot be justified. With the elimination of robotic assembly lines, however, comes an increased effort in the manufacturing of the parts that can effectively direct the self-assembly. This additional effort can be limited if conventional surface micromachining is used to realize the components, which was the case in our example.

Assembling and packaging of LEDs is conceptually interesting because it provides an example that has historically been realized with robotic assembly lines and wire bonders. It should be possible to extend this concept to systems where sensors or actuation elements are added to the assembly sequence. The use of nonconventional lithographic methods where the components can be patterned on all faces would provide even greater flexibility in the creation of three-dimensional systems that cannot be fabricated otherwise.

This work was supported by National Science Foundation Grant ECS-0300263.

1. Cohn, M. B., Bohringer, K. F., Noworolski, J. M., Singh, A., Keller, C. G., Goldberg, K. Y. & Howe, R. T. (1998) *Proc. SPIE Int. Soc. Opt. Eng.* **3512,** 2–16.
2. Clark, T. D., Tien, J., Duffy, D. C., Paul, K. E. & Whitesides, G. M. (2001) *J. Am. Chem. Soc.* **123,** 7677–7682.
3. Walz, M. (2003) *Circuits Assembly* **1,** 32–37.
4. Whitesides, G. M. & Grzybowski, B. (2002) *Science* **295,** 2418–2421.
5. Zhang, S. (2003) *Nat. Biotechnol.* **21,** 1171–1178.
6. Breen, T. L., Tien, J., Oliver, S. R. J., Hadzic, T. & Whitesides, G. M. (1999) *Science* **284,** 948–951.
7. Terfort, A. & Whitesides, G. M. (1998) *Adv. Mater.* **10,** 470–473.
8. Boncheva, M., Gracias, D. H., Jacobs, H. O. & Whitesides, G. M. (2002) *Proc. Natl. Acad. Sci. USA* **99,** 4937–4940.
9. Yeh, H. J. J. & Smith, J. S. (1994) *IEEE Photonics Technol. Lett.* **6,** 706–708.
10. Smith, J. S. & Yeh, H. J. J. (1998) U.S. Patent 5,824,186.
11. Bohringer, K. F., Srinivasan, U. & Howe, R. T. (2001) *Tech. Dig. MEMS*, 369–374.
12. Jacobs, H. O., Tao, A. R., Schwartz, A., Gracias, D. H. & Whitesides, G. M. (2002) *Science* **296,** 323–325.
13. Srinivasan, U., Liepmann, D. & Howe, R. T. (2001) *J. Microelectromech. Syst.* **10,** 17–24.
14. Gracias, D. H., Tien, J., Breen, T. L., Hsu, C. & Whitesides, G. M. (2000) *Science* **289,** 1170–1172.
15. Terfort, A., Bowden, N. & Whitesides, G. M. (1997) *Nature* **386,** 162–164.